ACS APPLIED ELECTRONIC MATERIALS

pubs.acs.org/acsaelm Article

Tailoring Electrical Stability of Indium Oxide Thin-Film Transistors via Solution Aging-Induced Defect Modulation

Juwon Kim, Seung-Jin Lee, Won-Ju Cho, and Hamin Park*

Cite This: ACS Appl. Electron. Mater. 2025, 7, 6187−6195 Read Online

ACCESS | Metrics & More | Article Recommendations | Supporting Information

ABSTRACT: The stability and performance of solution-processed indium oxide (InO) thin-film transistors (TFTs) are critically influenced by defect formation at the interface between the channel and the gate dielectric. This study comprehensively investigated the impact of solution aging time (0 min to 3 h) on the electrical and optoelectronic characteristics of InO TFTs, with an emphasis on defect-state modulation and charge-transport mechanisms. Changes in key TFT parameters, including the threshold voltage, subthreshold swing, and field-effect mobility, were analyzed as a function of solution aging duration. Bias-stress measurements confirm that positive bias stress-induced electron trapping and negative bias stress-driven oxygen vacancy ionization significantly affect device stability. The photoresponse of the InO films exhibits a nonmonotonic trend; the persistent photoconductivity increases for short aging times and diminishes on aging beyond 1 h, underscoring the dynamic evolution of defect states. X-ray photoelectron spectroscopy indicates that prolonged aging promotes the formation of stable In−O bonds while reducing the density of oxygen vacancies and hydroxyl-related defects, thereby improving electrical stability. These findings confirm a direct correlation between solution aging time and device reliability, offering valuable insights into optimizing the processing conditions of InO films for next-generation oxide-semiconductor electronics and optoelectronic applications.

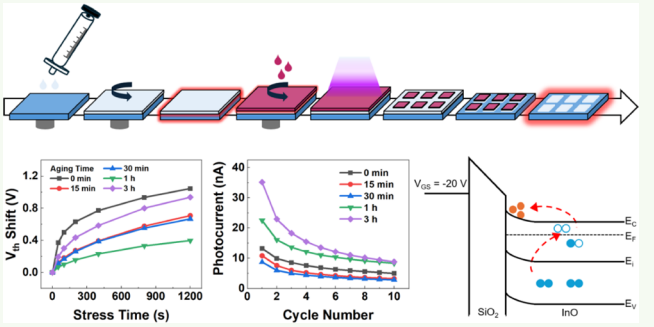

KEYWORDS: *indium oxide, thin-film transistor, solution process, aging time, stability, photoresponse*

INTRODUCTION

With rapid advancements in display technology, the demand for high-performance thin-film transistors (TFTs), which function as fundamental switching elements in modern display panels, has increased exponentially.[1,2] To ensure high resolution, rapid response, and excellent energy efficiency, the development of stable, high-mobility TFTs is essential. Amorphous silicon TFTs are widely used owing to their low-cost fabrication and excellent uniformity over large areas; however, low electron mobility limits their suitability for next-generation displays.[3] Low-temperature polycrystalline silicon TFTs show improved mobility and stability; however, their fabrication involves complex processing and high costs, limiting their suitability for large-scale production.[4]

Oxide-semiconductor TFTs have emerged as promising alternatives with high electron mobility, optical transparency, and low off-state current.[5,6] Among various oxide semiconductors, indium oxide (InO) is particularly promising because of its wide bandgap, high conductivity, and chemical stability, which make it suitable for transparent and flexible electronics.[7−9] Numerous fabrication techniques, such as reactive evaporation,[10] sputtering,[11] and atomic layer deposition,[12] have been used to produce high-quality InO thin films. However, these vacuum-based processes require expensive equipment and complex steps, limiting their scalability for cost-effective, large-area manufacturing.

Solution-based processing has gained prominence as an effective strategy for fabricating oxide-semiconductor TFTs because of its advantageous characteristics, including high compatibility with large-area deposition, process simplicity, and the ability to ensure low-cost mass production.[13−17] However, solution-processed InO thin films often show poor film uniformity, high defect density, and chemical instability, all of which adversely affect device performance and reliability. A critical factor influencing the properties of solution-processed films is the aging time of the precursor solution, which alters the solution chemistry, defect state formation, and overall film quality. Oxygen vacancies (V_O) and hydroxyl (−OH) groups, commonly introduced during solution processing, significantly influence the electrical stability and long-term reliability of solution-processed devices. Although oxygen vacancies can

Received: May 18, 2025
Revised: June 20, 2025
Accepted: June 24, 2025
Published: June 27, 2025

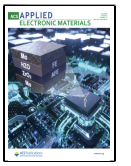

https://doi.org/10.1021/acsaelm.5c01021
ACS Appl. Electron. Mater. 2025, 7, 6187−6195

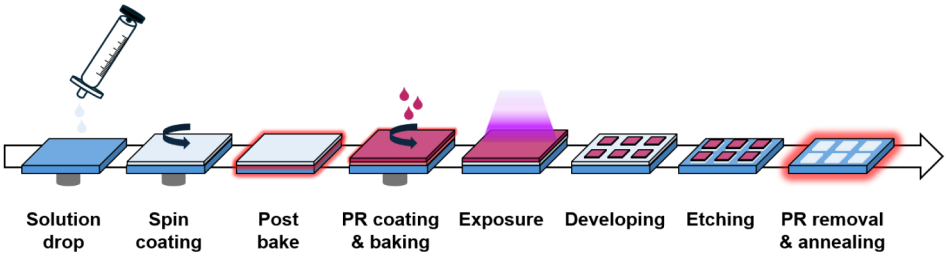

Figure 1. Schematics of fabricating solution-processed indium oxide thin-film transistors.

function as electron donors (enhancing carrier transport) at moderate concentrations, excess concentrations can introduce trap states that degrade mobility and cause threshold voltage (V_{th}) shifts over time.[18−20] Similarly, residual hydroxyl groups contribute toward defect formation and device instability, particularly under prolonged bias stress and UV illumination.[21,22]

To address these challenges and understand the underlying phenomena, this study systematically investigated the effect of solution aging time on the electrical and optical properties of solution-processed InO TFTs. The effect of different aging times (within 0 to 3 h) on defect formation, carrier transport, and device stability was analyzed using electrical measurements and material characterization techniques. X-ray diffraction (XRD) was used to examine the crystallinity of the InO films, whereas X-ray photoelectron spectroscopy (XPS) was used to investigate the changes in the chemical bonding states, particularly the presence of oxygen-related defects such as oxygen vacancies and hydroxyl groups. The influence of aging time on certain key TFT parameters (namely, the V_{th}, subthreshold swing (SS), and field-effect mobility (μ)) and device stability under positive bias stress (PBS) and negative bias stress (NBS) conditions were investigated to elucidate the specific roles of interface charge trapping and oxygen vacancy ionization. Furthermore, the photoresponse characteristics of the InO films were explored, focusing on persistent photoconductivity (PPC) behavior, to explore their potential for photodetector applications and understand the influence of aging time on PPC. By correlating the results of electrical, chemical, and optical analyses, this study provides a comprehensive understanding of the solution aging-based modulation of the performance and stability of solution-processed InO TFTs.

EXPERIMENTAL DETAILS

Solution Preparation. InO precursor solutions were prepared by dissolving indium nitrate hydrate ($In(NO_3)_3{\cdot}xH_2O$, 99.99%, Sigma-Aldrich) in 2-methoxyethanol to ensure a molar concentration of 0.08 M. The solution was stirred at 60 °C for 2 h to ensure complete dissolution. To investigate the effects of aging, five aliquots of the solution were stored for 0 min, 15 min, 30 min, 1 h, and 3 h before use. The storage conditions were 22 °C and 40−60% relative humidity, in glass vials sealed with Parafilm.

Device Fabrication. Bottom-gate and top-contact TFTs were fabricated on heavily doped n-type silicon substrates with a 90 nm thermally grown SiO_2 gate dielectric. Before film deposition, the substrates were cleaned with a piranha solution (H_2SO_4:H_2O_2 = 1:1 molar ratio) and dried with N_2 gas. The InO precursor solutions (aged as described above) were filtered through 0.2 μm poly tetrafluoroethylene syringe filters and spin-coated onto the substrates at 4000 rpm for 20 s. The films were preannealed at 180 °C for 10 min in air to remove most of the solvent. For patterning the InO active layer, photolithography and wet etching were performed using an AZ 5214E photoresist (Merck Performance Materials GmbH) and a 30:1 buffered oxide etchant solution, respectively. The etching was carried out for 10 s, yielding an etch rate of approximately 0.85 nm/s. Subsequently, postdeposition annealing was conducted in a furnace under an oxygen ambient at 400 °C for 30 min to enhance the crystallinity and electrical performance of the InO films. For device passivation, a thin poly(methyl methacrylate) (PMMA) layer was spin-coated and baked at 100 °C for 10 min. The resulting TFTs showed a channel width and length of 230 and 310 μm, respectively. The overall fabrication process is illustrated in Figure 1.

Electrical Characterization. The electrical properties of the InO TFTs were measured using a Keithley 2614B source meter in a dark ambient environment. The transfer characteristics (I_D−V_{GS}) were recorded at a drain-source voltage (V_{DS}) of 0.5 V while sweeping the gate-source voltage (V_{GS}) from −15 to +50 V. The output characteristics (I_D−V_{DS}) were measured at various fixed V_{GS} values. The bias stress stability was evaluated by applying a constant PBS (V_{DS} = 0.5 V, V_{GS} = 20 V) for 1200 s and NBS (V_{DS} = 0.5 V and V_{GS} = −20 V) for 1200 s. The V_{th} was extracted as the V_{GS} value at a normalized drain current of 10 nA. The SS was determined from the slope of the transfer curve in the subthreshold region (within I_D values of 100 pA and 1 nA). The field-effect mobility was extracted using the maximum transconductance method, defined as $\mu = (L \times g_{m\_max})/(W \times C_{ox} \times V_{DS})$, where L and W are the channel length and width, respectively; g_{m_max} is the maximum transconductance; and C_{ox} is the gate oxide capacitance per unit area.

Material Characterization. The crystallographic properties of the InO films were examined by XRD (Rigaku D/MAX-2500/PC) with a Cu Kα radiation source ($\lambda \approx 1.54$ Å) at 60 kV and 300 mA. The surface chemical composition and bonding states were analyzed by XPS (ULVAC-PHI 5000 VersaProbe, Al Kα source) with a pass energy of 40 eV and 10 μm beam spot. The XPS profiles were calibrated using the C 1s peak (284.8 eV) as a reference.

Photoresponse Measurement. Photodetector measurements were carried out using a DYMAX BlueWave LED VisiCure UV source (405 nm wavelength, intensity ~6.5 mW·cm^{-2}). For each device, the channel was illuminated with UV light for 5 s and the decay of the drain current was monitored in the dark for 55 s. Using this procedure, both the immediate photoresponse and the persistent photoconductivity behavior after the light was turned off could be evaluated.

RESULTS AND DISCUSSION

The electrical characteristics and stability of the InO TFTs were found to depend strongly on the aging time of the precursor solution. Devices were fabricated using solutions aged for 0 min, 15 min, 30 min, 1 h, and 3 h to systematically investigate the effect of aging time on device performance. First, the structural qualities of the InO films were evaluated. The XRD patterns of all the fabricated devices (Figure S1) contain the same prominent In_2O_3 (222) diffraction peak, indicating that the crystalline phase and grain orientation of the InO film remain consistent, regardless of solution aging.[9] Thus, no significant changes in film crystallinity were observed as a function of the aging time.

https://doi.org/10.1021/acsaelm.5c01021
ACS Appl. Electron. Mater. 2025, 7, 6187−6195

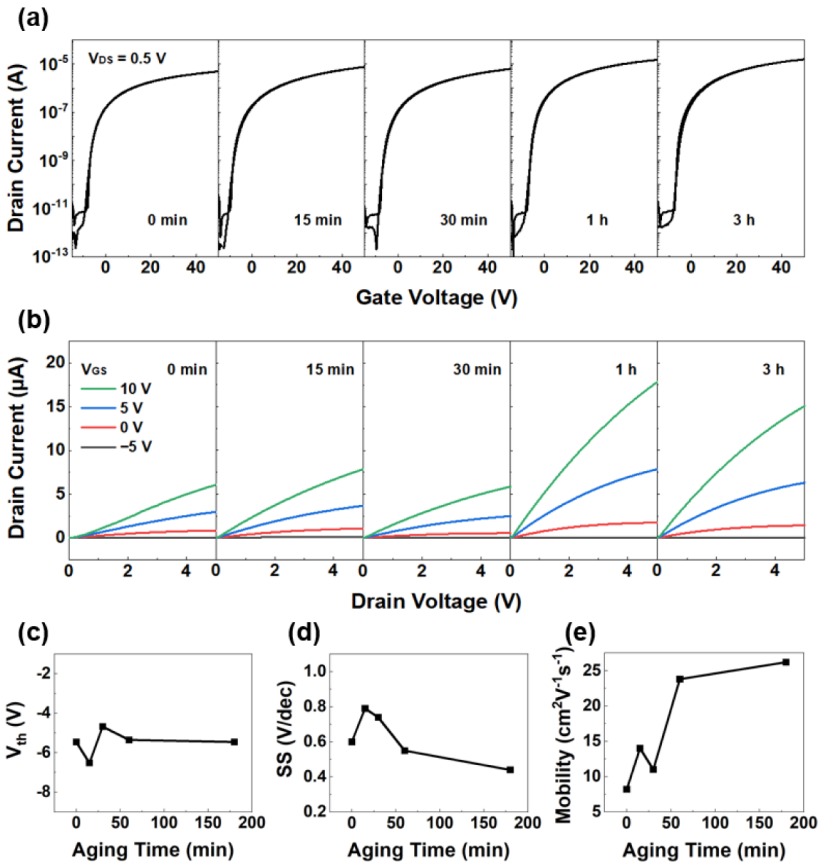

Figure 2. (a) Transfer and (b) output characteristics of InO TFTs fabricated with solutions aged for 0 min, 15 min, 30 min, 1 h, and 3 h. (c) Extracted threshold voltage (V_{th}), (d) subthreshold swing (SS), and (e) field-effect mobility (μ) as a function of aging time.

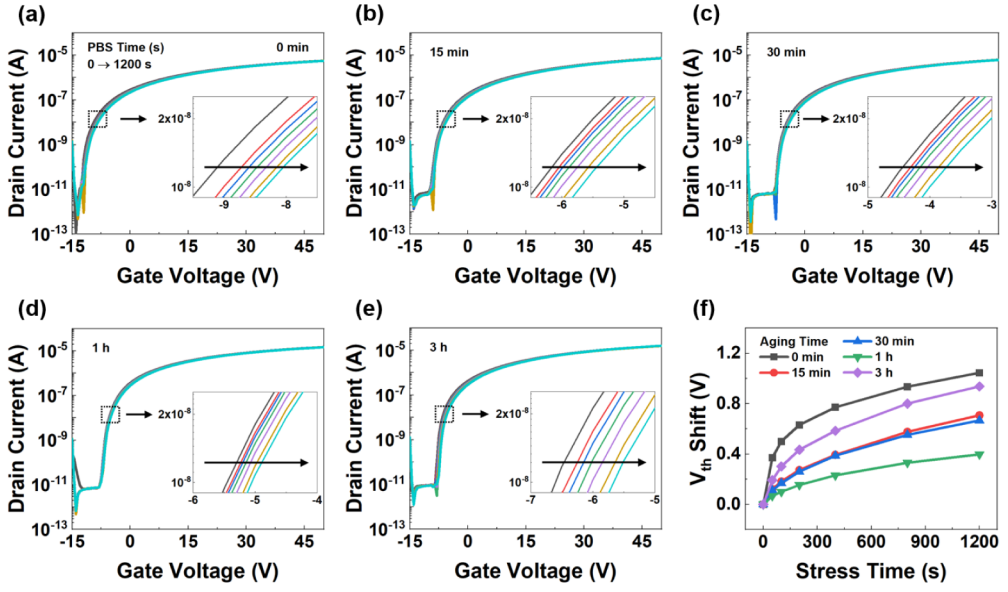

Figure 3. Time evolution of transfer characteristics under a 1200 s positive bias stress (PBS) for InO TFTs with solution aging times of (a) 0 min, (b) 15 min, (c) 30 min, (d) 1 h, and (e) 3 h. (f) Corresponding V_{th} shift (ΔV_{th}) as a function of stress time for each aging condition.

Figure 2 summarizes the basic transistor characteristics of the devices fabricated using solutions aged for different durations of time. Figure 2a shows the transfer characteristics measured at a V_{DS} of 0.5 V. All devices exhibit typical n-type behavior with negligible hysteresis, indicating stable operation without significant charge trapping at the semiconductor/dielectric interface. Figure 2b shows the output characteristics of the same devices; the linear region of the output curves do not indicate current suppression at a low V_{DS}, confirming that the conduction channel remains stable and ohmic under the measurement conditions. This reliable behavior is consistently observed across multiple devices. Figure S2 shows transfer

https://doi.org/10.1021/acsaelm.5c01021
ACS Appl. Electron. Mater. 2025, 7, 6187−6195

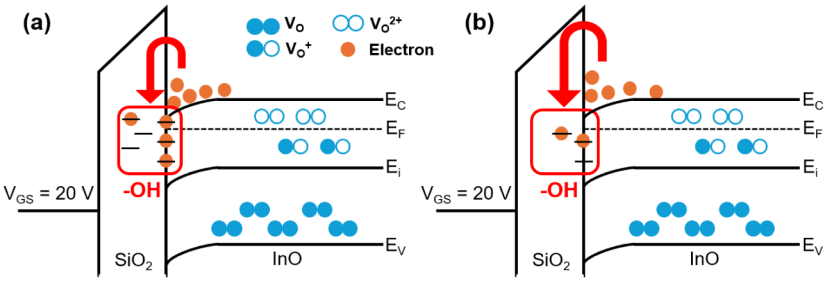

Figure 4. Energy band diagrams (conduction band edge) near the channel/dielectric interface under PBS showing two scenarios: (a) a device with a high trap-state density (for example, a device manufactured using solutions aged for 0 min or 3 h) containing many trapped electrons, and (b) a device with a low trap-state density (for example, a device manufactured using solutions aged for 15 min or 1 h) containing comparatively few trapped electrons. Trapped electrons cause a pronounced positive V_{th} shift and reduce channel conductivity in scenario (a) much more than in scenario (b).

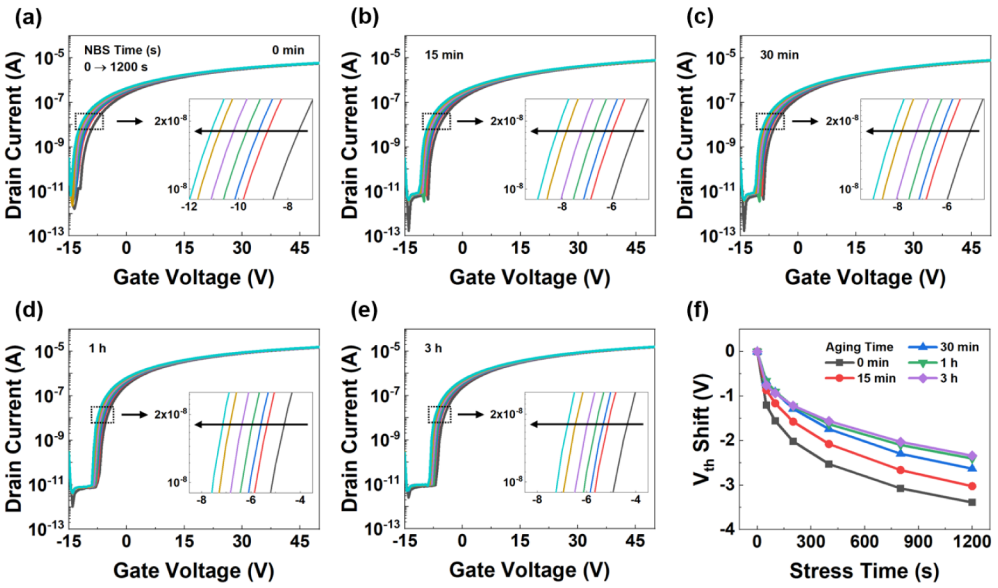

Figure 5. Time evolution of transfer characteristics under a 1200 s negative bias stress (NBS) for InO TFTs manufactured using solutions aged for (a) 0 min, (b) 15 min, (c) 30 min, (d) 1 h, and (e) 3 h. (f) Corresponding V_{th} shift (ΔV_{th}) versus stress time under NBS for each aging time.

curves for five separate devices, all of which exhibit similar performance. This uniformity indicates good process reproducibility and device stability under different aging conditions..

Figure 2c,d, and e quantifies the evolution of key transistor parameters (V_{th}, SS, and μ, respectively) with aging time. Notably, the V_{th} and SS values remain relatively unchanged with increasing aging time, implying that the turn-on voltage and subthreshold slope are negligibly affected by solution aging within the time range used for experimentation. In contrast, the μ value increases significantly for longer aging times; devices fabricated using solutions aged for 3 h show a μ value of 26 cm^2 V^{-1} s^{-1}. This mobility enhancement can be attributed to changes in the defect chemistry of the system. The mobility is proposed to be primarily influenced by intrinsic oxygen vacancies and residual organic species from the precursor. Oxygen vacancies function as electron donors, increasing the carrier concentration and creating percolation pathways, thereby increasing the mobility.[23,24] However, excess oxygen vacancies result in the formation of trap states that scatter charge carriers, ultimately reducing the mobility. Residual organic contaminants or hydroxyl species in the film (introduced during solution processing) can function as electron-trap sites that diminish the mobility through electron capture.[25] The balance and evolution of these two types of defects with aging time likely lead to the observed mobility trend, which is elucidated further based on the XPS results observed in this study.

PBS tests were used to evaluate the stability of the TFTs under prolonged electrical stress. Under a constant positive gate bias, electron trapping at the interface and oxide defect states can induce a positive shift in the V_{th} over time, which indicates the density of the trap states. Figure 3a–e shows the evolution of the transfer curves for devices fabricated using solutions aged for 0 min, 15 min, 30 min, 1 h, and 3 h, respectively, under 1200 s of PBS. Figure 3f, which plots the ΔV_{th} as a function of stress time for each aging condition, indicates that all devices exhibit a gradual positive shift in V_{th} with increasing stress time, with the magnitude of the shift varying depending on the aging time. Notably, the devices fabricated using solutions aged for 0 and 3 h show larger V_{th} shifts under PBS than those aged for 15–60 min; a smaller shift indicates higher stability. These results suggest that the trap-state density, which is responsible for PBS instability, is higher at the two extremes of aging (no aging and long aging) and lower at intermediate aging times. PBS-induced instabilities can be primarily attributed to electron trapping in preexisting defect states at the channel/gate interface or within the gate dielectric.[26–28] Because the positive gate bias bends

https://doi.org/10.1021/acsaelm.5c01021
ACS Appl. Electron. Mater. 2025, 7, 6187–6195

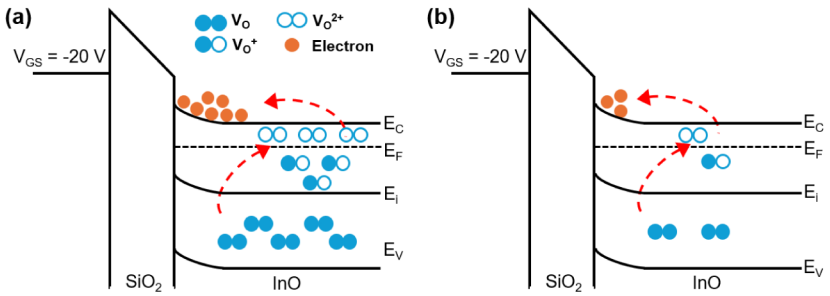

Figure 6. Energy-band diagrams under NBS highlighting the role of oxygen vacancies: (a) for devices with a high oxygen-vacancy density (such as devices manufactured using samples with no aging) in which many oxygen vacancies are ionized under negative bias, resulting in the injection of a significant number of electrons (blue "e^-") into the channel, leading to a large negative V_{th} shift, and (b) for a device with a low oxygen-vacancy density (such as devices manufactured using samples subjected to prolonged aging) in which few vacancies are available for ionization, resulting in the addition of few electrons to the channel, finally leading to a minimal V_{th} shift.

the conduction band downward at the interface, it facilitates electron trapping in these defect states, reducing the number of free carriers in the channel and causing V_{th} to shift positively. Such trapped electrons also lead to a reduction in the drain current because they no longer contribute toward conduction.[29,30]

The schematic energy-band diagram in Figure 4 shows the influence of trap states on the device under PBS for two representative cases: (a) when the device contains a high trap-state density (Figure 4a, characteristic of devices manufactured using the 0 min and 3 h aged samples) and (b) when the device contains a low trap-state density (Figure 4b, characteristic of devices manufactured using samples aged for intermediate aging times, such as 15 min or 1 h). Under a positive gate bias, the bands bend downward, and a significant number of electrons are captured by the trap states near the interface in the high-trap-state density case. The accumulation of trapped charges in scenario (a) leads to a more pronounced positive V_{th} shift and greater current suppression than in scenario (b), where fewer trap states are available for electron capture, resulting in a relatively small V_{th} shift. Notably, devices derived from both the 0 min and 3 h aged samples show the largest V_{th} shifts, indicating that trap-state formation as a function of aging does not follow a simple monotonic trend. This nonlinearity suggests the presence of multiple competing factors in defect creation and annihilation during the solution-aging process. For example, the oxygen vacancy concentration initially decreases on aging due to a reduction in traps; however, other defects or adsorbates accumulate on prolonged aging, increasing the overall trap density. Nevertheless, besides limiting the instantaneous electron mobility in the system, the presence of abundant trap states (as observed in samples subjected to extreme aging) reduces the long-term reliability of the device. Therefore, trap-state minimization through processing control is critical for improving device stability.

NBS tests on the same set of devices were used to probe the role of oxygen vacancies in device stability further. Under a negative gate bias, some oxygen vacancies can become ionized, thereby releasing free electrons into the channel. Additional free electrons increase the channel conductivity, typically causing a negative shift in V_{th}. Figure 5a–e shows transfer curves over 1200 s under NBS for devices manufactured using solutions aged for 0–3 h. As expected, all devices exhibit a negative shift in V_{th} under NBS. However, similar to the PBS case, the magnitude of this shift is strongly dependent on the aging time. Figure 5f plots the V_{th} shift as a function of stress time for each aging condition under NBS. We observed that devices manufactured using freshly prepared solution (0 min) show the largest negative ΔV_{th} (i.e., the most instability), whereas devices manufactured using the longest-aged solution (3 h) show a noticeably smaller shift. The primary mechanism for the NBS-induced negative V_{th} shift is the ionization of oxygen vacancies near the interface: initially, neutral oxygen-vacancy sites (V_O) become positively charged (V_O^+) under negative bias, releasing electrons into the conduction band. These extra electrons temporarily increase the carrier density, shifting the threshold in the negative direction. The 0 min sample likely contains the highest concentration of oxygen vacancies; therefore, it produces the largest pool of free electrons upon bias stress, and hence, the largest V_{th} shift. Conversely, the 3 h aged sample likely contains few oxygen vacancies that can be ionized, resulting in a small shift.

The trend of decreasing NBS instability with increasing aging times indicates that prolonged aging effectively reduces the concentration of easily ionizable oxygen vacancies in the film. As aging progresses, an increasing number of indium atoms attain full oxygen coordination (as suggested by XPS analysis), resulting in the presence of fewer oxygen vacancy defects that can contribute electrons under stress. Additionally, with fewer oxygen vacancies available for ionization, fewer excess carriers are introduced, and those introduced can recombine more readily, mitigating the overall effect on V_{th}. Figure 6 illustrates this concept. Panel (a) shows that devices with a high oxygen-vacancy density (such as systems manufactured using samples with no aging) exhibit a large negative V_{th} shift under NBS owing to the abundant release of electrons from ionized vacancies. Panel (b) shows that devices with a significantly low oxygen-vacancy density (such as those manufactured using solutions subjected to prolonged aging) exhibit a small V_{th} shift owing to the release of few electrons under NBS. Thus, extended aging appears to stabilize the device against NBS by decreasing the density of oxygen vacancy donors. This improvement in NBS stability complements the PBS results, indicating that moderate aging yields the most electrically stable devices. Therefore, tuning the oxygen-vacancy population through processing is crucial for enhancing long-term device performance. To comprehensively evaluate device stability and underlying defect mechanisms, we performed both PBS and NBS tests, each targeting distinct types of electrically active defects. PBS primarily probes the trapping of electrons in preexisting trap states, such as those associated with hydroxyl groups or interface-related defects near the channel/dielectric interface. In contrast, NBS is sensitive to the ionization of oxygen vacancies within the InO

https://doi.org/10.1021/acsaelm.5c01021
ACS Appl. Electron. Mater. 2025, 7, 6187–6195

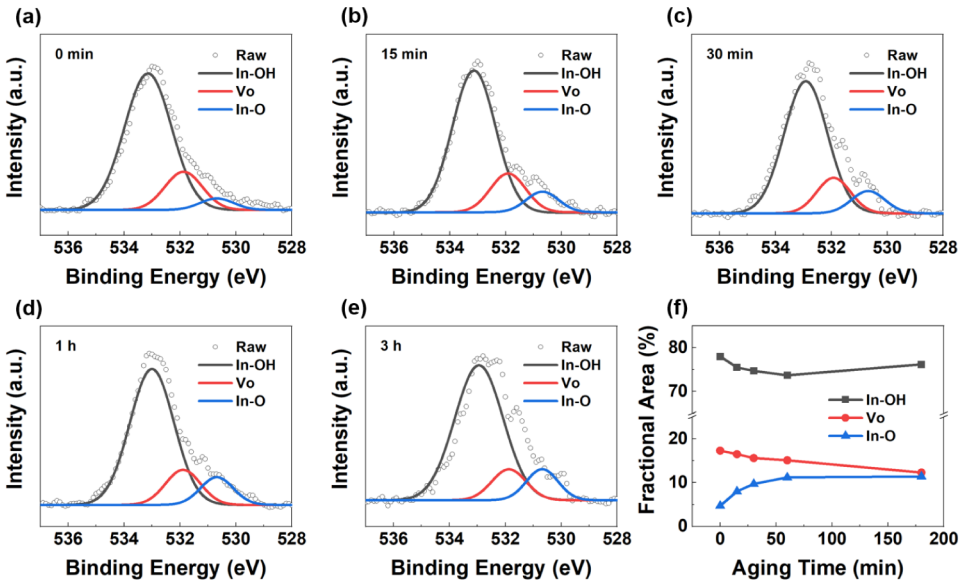

Figure 7. XPS O 1s spectra for InO films manufactured using solutions with aging times of (a) 0 min, (b) 15 min, (c) 30 min, (d) 1 h, and (e) 3 h. The spectra are deconvoluted into contributions from lattice oxygen in In−O bonds (blue peak, ∼530.7 eV), oxygen vacancies (V_O, red peak, ∼531.9 eV), and In−OH groups (black peak, ∼533.1 eV). (f) Relative percentages of In−O (blue), V_O (red), and In−OH (black) components as a function of aging time showing that prolonged aging increases the In−O fraction while reducing the oxygen vacancy and hydroxyl content of the system.

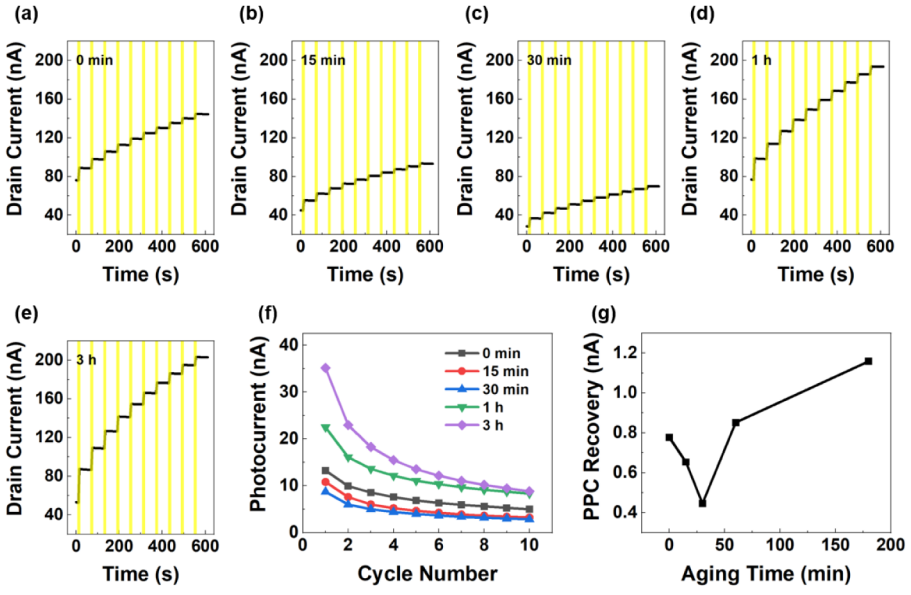

Figure 8. Drain current response under 405 nm UV illumination (yellow-shaded interval indicates a 5 s light pulse) and subsequent decay in the dark for devices manufactured using solutions aged for (a) 0 min, (b) 15 min, (c) 30 min, (d) 1 h, and (e) 3 h. (f) Photocurrent amplitude (steady-state current under illumination) as a function of aging time, which initially decreases and then recovers over prolonged aging. (g) Persistent photoconductivity (PPC) results, represented by the percentage of photocurrent remaining ∼55 s after the light is turned off as a function of aging time. Devices derived from solutions aged for ∼15−30 min exhibit the highest PPC, whereas those derived from solutions subjected to no or prolonged aging show a significantly low PPC.

film, which act as donor-like defects and release electrons under negative gate bias. Therefore, the combined use of PBS and NBS provides complementary insights into trap-mediated and donor-mediated instability mechanisms, enabling a comprehensive understanding of the defect behavior as it evolves with solution aging.

XPS analysis was used to elucidate the chemical changes determining the electrical behavior of InO films derived from solutions aged for different times. Figure 7a−e shows the XPS O 1s spectra for samples aged from 0 min to 3 h. Each O 1s spectrum was deconvoluted into three components corresponding to different oxygen-bonding environments: the peak near 530.7 eV is attributed to lattice oxygen in the In−O bonds (i.e., O^{2-} in the crystalline InO matrix), the peak around 531.9 eV is associated with oxygen vacancies (i.e., oxygen in oxygen-deficient environments), and the peak around 533.1 eV is assigned to oxygen in hydroxyl groups (In−OH) or in absorbed water-related species. The relative areas of these

https://doi.org/10.1021/acsaelm.5c01021
ACS Appl. Electron. Mater. 2025, 7, 6187−6195

components are shown in Figure 7f. With increasing aging time increases, the fraction of the lattice O (In−O) component steadily increases, whereas that of the oxygen-vacancy component decreases. For example, among the tested systems, the film derived from the 0 min aged solution shows the most intense oxygen-vacancy signal. Notably, the intensity of this signal reduces significantly for films derived from the solution subjected to 3 h of aging, the spectrum of which contains an intense In−O component. This, longer aging results in the formation of a fully oxidized indium oxide network with fewer vacancy defects, which is expected to be chemically and electrically stable.[31] Furthermore, a slight reduction in the intensity of the hydroxyl-related O 1s component is observed with increasing aging (the In−OH peak fraction is somewhat lower for the 3 h aged sample than the 0 min aged sample). The presence of −OH in the films likely originates from residual solvent or moisture incorporated into the film during the solution process; these hydroxyl groups can function as electron-trapping defect states because of their polar nature.[32] Thus, the XPS results of this study corroborate with the electrical findings: solution aging enables complete oxide formation (with the formation of fewer V_O and −OH defects), consistent with the reduction in V_{th} shifts and enhancement in stability with increasing aging, especially in the intermediate-aging range.

Notably, XRD (Figure S1) indicated no significant changes in crystallinity with aging, implying that the device-behavior improvements on aging can be largely attributed to defect-chemistry changes rather than crystalline-structure transitions. Therefore, by reducing the density of oxygen vacancies and hydroxyl-related defects (as evidenced by XPS), the aging process improves the interface quality and intrinsic film stability without altering the basic InO crystal structure. Under PBS, fewer −OH trap sites in longer-aged films result in the trapping of fewer electrons, finally leading to a small positive ΔV_{th}; and under NBS, a lower vacancy density indicates the generation of fewer electrons, leading to a small negative ΔV_{th}. These chemical insights highlight the importance of controlling solution chemistry to tailor the defect landscape in oxide-semiconductor films.

Finally, the optoelectronic behavior of the InO films was examined via UV photoresponse and PPC measurements of devices manufactured using solutions aged for different times. These measurements provide an additional perspective on the evolution of defect states because photoexcited carrier dynamics are highly sensitive to trapping and recombination centers within the metal oxide channel. PPC has been widely reported in various oxide semiconductors, including InO, InGaZnO, and ZnO, and is typically attributed to oxygen vacancies and metastable donor-like defects that trap photogenerated carriers and gradually release them after illumination is removed.[33−36] Figure 8a−e shows the transient drain-current responses of representative devices during and after 5 s of UV illumination (the yellow shaded region indicates when the UV lamp is on) for aging times of 0 min, 15 min, 30 min, 1 h, and 3 h. Both the magnitude of the photocurrent and the persistence of the current after the light is turned off differ distinctly for the tested devices. For devices manufactured using solutions with no or short aging (0−30 min), the peak photocurrent under illumination is relatively high for 0 min, decreases as the aging time increases to 30 min, and increases at 1 and 3 h of aging, nearly recovering or even exceeding the initial value. This nonmonotonic trend is summarized in Figure 8f, which plots the steady-state photocurrent (including the current level at the end of 5 s illumination) as a function of aging time. This behavior is interpreted in terms of the defect landscape. For very short aging times, a high density of oxygen vacancies provides a large number of photogenerated carriers, resulting in a high initial photocurrent. However, with ∼30 min of aging, some of these vacancies become passivated or the film network become rigid (with increased In−O bonding), resulting in fewer available carriers under illumination, leading to a lower photocurrent. Additionally, shorter-aged samples contain abundant trap sites (such as −OH or other defects) that rapidly capture photocarriers, facilitating recombination rather than conduction; this leads to a reduction in the photocurrent.[37] On extending aging further (≥1 h), certain In−O bonds start to dissociate or additional oxygen vacancies are introduced into the system, reincreasing carrier generation. Thus, long-aged solutions produce films with a moderate density of oxygen vacancies that can generate electrons under illumination but contain a relatively low trap density for these carriers; thus, the photocurrent increases on 1 and 3 h aging. Eventually, under prolonged illumination, the photocurrent reaches a saturation point in each case, indicating a balance between photogeneration and recombination..

PPC behavior (i.e., the current-decay behaviors after the light is turned off) varies with aging. Figure 8a−e indicates that a significant portion of the photocurrent persists, even tens of seconds after illumination, for the 0 and 15 min aged samples, whereas the current decreases rapidly for the 3 h aged sample. Figure 8g shows the quantification of the PPC by comparing the residual current at 55 s (end of the measurement) with the initial dark current for each device. The PPC is most pronounced for intermediate aging (devices manufactured using solutions aged for ∼15 to 30 min), which show the highest residual current ratio, whereas devices derived from solutions aged for 0 and 3 h show a low PPC. This trend can be rationalized as follows: in the early aging phase, multiple oxygen vacancies provide carriers under illumination, which are trapped by the multiple trap sites in the system. When the light is turned off, these traps gradually release the carriers, leading to prolonged photoconductivity. On ∼15−30 min of aging, a reduction in vacancy density (and some trap passivation) results in fewer free carriers in the device along with effective carrier trapping, leading to extended decay and a high PPC. However, long-aged films (≥1 h) contain fewer traps for carrier capture owing to significant defect elimination; although these films show an intense photoresponse, the carriers recombine or get recaptured rapidly when illumination ceases, leading to rapid decay and a low PPC. In summary, reducing trap states via aging improves the photoresponse speed but shortens the persistence, whereas increasing the trap density extends the PPC but can suppress the instantaneous photocurrent. These observations highlight the trade-off in defect engineering for optoelectronic devices; designing systems with optimal density and defect type can ensure a balance between a strong photoresponse and a controlled PPC, enabling the fabrication of devices depending on the intended application.

Overall, the results of photoresponse and PPC analyses confirm that the precise control of the solution aging time is necessary for tuning the defect landscape for specific device performance. The contrasting behavior of devices based on solutions subjected to short and long aging emphasizes the importance of defect engineering; by adjusting processing

https://doi.org/10.1021/acsaelm.5c01021
ACS Appl. Electron. Mater. 2025, 7, 6187−6195

conditions such as aging, charge trapping and carrier-release dynamics can be modulated to either favor rapid photoresponse or prolonged photoconductivity. Here, devices based on solutions subjected to moderate aging times showed balanced attributes, i.e., an acceptable photoresponse and manageable PPC, consistent with the trend that these conditions yield the most electrically stable TFT operation. By tuning the defect landscape through controlled aging, the device reliability and performance can be significantly enhanced for use in next-generation oxide-semiconductor electronics and optoelectronics.

CONCLUSION

This work comprehensively examines the influence of solution aging time on the defect structure and performance of InO TFTs. The results of this study confirm that aging time is a pivotal factor in modulating defect states that can be used for tuning device behavior. According to electrical measurements, V_{th} and SS remain fairly stable across the range of aging times used for analysis in this study, whereas the field-effect mobility approximately doubles with increasing aging time owing to a reduction in scattering centers. Bias stress tests (PBS/NBS) confirmed that electron traps and ionized oxygen vacancies are the key contributors toward V_{th} instability; devices derived from solutions subjected to extremely short or long aging times exhibit larger V_{th} shifts than those derived from solutions subjected to intermediate aging, which exhibit relatively stable operation. Structural analysis via XRD indicated insignificant crystallographic changes with aging, suggesting that the performance differences between devices derived from solutions aged for different times can be attributed primarily to chemical defects. According to XPS analysis, prolonged aging promotes the formation of In−O bonds, resulting in highly oxidized films, and reduces the concentration of oxygen vacancies and −OH defects, which can be correlated with the improved stability of the system. In optoelectronic characterization experiments, the photoresponse and PPC showed nonmonotonic behavior; moderate aging times optimize the trade-off between immediate photoconductivity and PPC, whereas no or overaging leads to imbalances. Collectively, these findings highlight the possibility of tailoring the defect landscape within InO films, enhancing their electrical stability without sacrificing mobility, and tuning their photoresponse characteristics by precisely controlling the precursor solution aging duration. The insights obtained in this study provide a pathway for enhancing the electrical and optical stability of InO TFTs through controlled defect modulation, while also highlighting promising opportunities to apply this strategy to flexible electronics and integrated optoelectronic systems, such as UV photodetectors and transparent sensors. Future work may explore its applicability to bendable and stretchable substrates and evaluate its compatibility with large-area manufacturing processes.

ASSOCIATED CONTENT

Supporting Information

The Supporting Information is available free of charge at https://pubs.acs.org/doi/10.1021/acsaelm.5c01021.

X-ray diffraction patterns, $I-V$ characteristics of independent InO thin-film transistors (PDF)

AUTHOR INFORMATION

Corresponding Author

Hamin Park − *Department of Electronic Engineering, Kwangwoon University, Seoul 01897, Republic of Korea;* orcid.org/0000-0002-5354-3573; Email: parkhamin@kw.ac.kr

Authors

Juwon Kim − *Department of Electronic Engineering, Kwangwoon University, Seoul 01897, Republic of Korea*

Seung-Jin Lee − *Department of Electronic Materials Engineering, Kwangwoon University, Seoul 01897, Republic of Korea*

Won-Ju Cho − *Department of Electronic Materials Engineering, Kwangwoon University, Seoul 01897, Republic of Korea*

Complete contact information is available at: https://pubs.acs.org/10.1021/acsaelm.5c01021

Notes

The authors declare no competing financial interest.

ACKNOWLEDGMENTS

This work was supported by the National Research Foundation of Korea (NRF), funded by the Ministry of Science and ICT (No. RS-2024-00335269) and by the Ministry of Education (No. RS-2018-NR031063). This work was also supported by K-CHIPS (No. RS-2023-00237548 (23015-30FC, 1415187530)) funded by the Ministry of Trade, Industry and Energy of Korea and by the Research Grant of Kwangwoon University in 2025.

REFERENCES

(1) Liang, Z. H.; Wu, W. J.; Fang, Z. Q.; Deng, Z. E.; Fu, X.; Ning, H. L.; Luo, D. X.; Zhu, Z. N.; Yao, R. H.; Peng, J. B. A review of doped metal oxide semiconductors in the stability of thin film transistors. *J. Alloys Compd.* **2025**, *1010*, 177434.

(2) Park, J. S.; Maeng, W. J.; Kim, H. S.; Park, J. S. Review of recent developments in amorphous oxide semiconductor thin-film transistor devices. *Thin Solid Films* **2012**, *520* (6), 1679−1693.

(3) Nomura, K.; Ohta, H.; Takagi, A.; Kamiya, T.; Hirano, M.; Hosono, H. Room-temperature fabrication of transparent flexible thin-film transistors using amorphous oxide semiconductors. *Nature* **2004**, *432* (7016), 488−492.

(4) Sheng, J. Z.; Lee, J. H.; Choi, W. H.; Hong, T.; Kim, M.; Park, J. S. Review Article: Atomic layer deposition for oxide semiconductor thin film transistors: Advances in research and development. *J. Vac. Sci. Technol., A* **2018**, *36* (6), 060801.

(5) Fortunato, E.; Barquinha, P.; Martins, R. Oxide Semiconductor Thin-Film Transistors: A Review of Recent Advances. *Adv. Mater.* **2012**, *24* (22), 2945−2986.

(6) Zhao, T. S.; Zhao, C.; Zhang, J. F.; Mitrovic, I. Z.; Lim, E. G.; Yang, L.; Song, T.; Zhao, C. Z. Enhancement on the performance of eco-friendly solution-processed InO/AlO thin-film transistors via lithium incorporation. *J. Alloys Compd.* **2020**, *829*, 154458.

(7) Han, S. Y.; Herman, G. S.; Chang, C. H. L.-T. High-Performance, Solution-Processed Indium Oxide Thin-Film Transistors. *J. Am. Chem. Soc.* **2011**, *133* (14), 5166−5169.

(8) Li, X. Y.; Cheng, J.; Gao, Y. F.; Li, M.; Kuang, D.; Li, Y.; Xue, J. S.; Zhang, T.; Yu, Z. N. Impact of NH3 plasma treatment for solution-processed indium oxide thin-film transistors with low thermal budget. *J. Alloys Compd.* **2020**, *817*, 152720.

(9) Hong, T.; Kim, K.; Choi, S. H.; Lee, S. H.; Han, K. L.; Lim, J. H.; Park, J. S. S. Optical, and Electrical Properties of InOX Thin Films Deposited by Plasma-Enhanced Atomic Layer Deposition for Flexible

Device Applications. *ACS Appl. Electron. Mater.* **2022**, *4* (6), 3010−3017.
(10) Dhananjay; Chu, C.-W. Realization of In2O3 thin film transistors through reactive evaporation process. *Appl. Phys. Lett.* **2007**, *91* (13), 132111.
(11) Guo, S.; Diyatmika, W.; Unutulmazsoy, Y.; Yang, L.; Dai, B.; Xu, L. G.; Han, J. C.; Ralchenko, V.; Anders, A.; Zhu, J. Q. High-quality transparent conductive indium oxide film deposition by reactive pulsed magnetron sputtering: Determining the limits of substrate heating. *Appl. Surf. Sci.* **2022**, *585*, 152604.
(12) Ryu, S.-H.; Hong, T.; Choi, S.-H.; Yeom, K.; Ryu, D. W.; Seok, J. H.; Park, J.-S. Tailoring indium oxide film characteristics through oxygen reactants in atomic layer deposition with highly reactive liquid precursor. *Appl. Surf. Sci.* **2024**, *664*, 160271.
(13) Shan, F.; Lee, J. Y.; Tarsoly, G.; Zhao, H. L.; Wang, X. L.; Anvar, T.; Yoo, S.; Kim, S. J. Enhancement of Electrical Stability in Solution Processed In2O3 TFT by an Oxygen Plasma-Assisted Treatment. *IEEE Trans. Electron Devices* **2023**, *70* (11), 5678−5684.
(14) Wang, X. L.; Zhao, H. L.; Shan, F.; Shi, S. K.; Lee, J. Y.; Tarsoly, G.; Kim, S. J. Aqueous solution-processed In2O3 TFTs using focused plasma in gas mixtures. *Appl. Surf. Sci.* **2024**, *669*, 160576.
(15) Diao, Z. T.; Gong, T. Z.; Li, X. Y.; Hu, Y. B.; Hu, W. Solution-Processed Perovskite and Oxide-Semiconductor Heterostructure Construction for a High-Performance Ultraviolet Photodetector. *ACS Appl. Electron. Mater.* **2024**, *6* (4), 2316−2322.
(16) Lee, J. Y.; Tarsoly, G.; Wang, X. L.; Zhao, H. L.; Heo, K. J.; Kim, S. J. Engineering a Solution-Processed In2O3 TFT With Improved Ambient Stability via MoO3 Doping. *IEEE Trans. Electron Devices* **2024**, *71* (3), 1946−1950.
(17) Guo, M.; Wu, J. T.; Ou, H.; Xie, D. Y.; Zhu, Q. J.; Huang, Y.; Wang, M. Y.; Liang, L. Y.; Liang, X. C.; Liu, F. J.; Ning, C.; Lu, X. B.; Cao, H. T.; Yuan, G. C.; Liu, C. Comparative Study of Indium Oxide Films for High-Mobility TFTs: ALD, PLD and Solution Process. *Adv. Electron. Mater.* **2025**, *11* (2), 2400145.
(18) Hwang, D. K.; Misra, M.; Lee, Y. E.; Baek, S. D.; Myoung, J. M.; Lee, T. The role of Ar plasma treatment in generating oxygen vacancies in indium tin oxide thin films prepared by the sol-gel process. *Appl. Surf. Sci.* **2017**, *405*, 344−349.
(19) He, F. C.; Qin, Y.; Wang, Y. F.; Lin, Z. H.; Su, J.; Zhang, J. C.; Chang, J. J.; Hao, Y. Aqueous Solution Derived Amorphous Indium Doped Gallium Oxide Thin-Film Transistors. *IEEE J. Electron Devices Soc.* **2021**, *9*, 373−377.
(20) Lee, P.; Le, M. N.; Kim, G.; Kwon, S. M.; Jo, J. W.; Kim, J.; Kim, Y. H.; Park, S. K.; Ahn, K.; Kim, M. G. Efficient Oxygen-Vacancy Suppression and Electrical Stabilization of Solution-Processed In2O3:Q (Q = S, Se) Thin-Film Transistor with Chalcogen Alloying. *Adv. Electron. Mater.* **2022**, *8* (7), 2101250.
(21) Jeon, J. K.; Um, J. G.; Lee, S.; Jang, J. Control of O-H bonds at a-IGZO/SiO2 interface by long time thermal annealing for highly stable oxide TFT. *AIP Adv.* **2017**, *7* (12), 125110.
(22) Kim, B. S.; Kim, H. J. Influence of Annealing on Solution-Processed Indium Oxide Thin-Film Transistors Under Ambient Air and Wet Conditions. *IEEE Trans. Electron Devices* **2016**, *63* (9), 3558−3561.
(23) Kamiya, T.; Nomura, K.; Hosono, H. Electronic Structures Above Mobility Edges in Crystalline and Amorphous In-Ga-Zn-O: Percolation Conduction Examined by Analytical Model. *J. Dispersion Technol.* **2009**, *5* (12), 462−467.
(24) Lee, S.; Ghaffarzadeh, K.; Nathan, A.; Robertson, J.; Jeon, S.; Kim, C.; Song, I. H.; Chung, U. I. Trap-limited and percolation conduction mechanisms in amorphous oxide semiconductor thin film transistors. *Appl. Phys. Lett.* **2011**, *98* (20), 203508.
(25) Kim, J. H.; Park, E. K.; Kim, M. S.; Cho, H. J.; Lee, D. H.; Kim, J. H.; Khang, Y.; Park, K.; Kim, Y. S. Bias and illumination instability analysis of solution-processed a-InGaZnO thin-film transistors with different component ratios. *Thin Solid Films* **2018**, *645*, 154−159.
(26) Choi, S.; Choi, S. J.; Kim, D. H.; Park, S.; Kim, J.; Seo, Y.; Shin, H. J.; Jeong, Y. S.; Bae, J. U.; Oh, C. H.; Kim, D. M. Positive Bias Stress Instability of InGaZnO TFTs With Self-Aligned Top-Gate Structure in the Threshold-Voltage Compensated Pixel. *IEEE Electron Device Lett.* **2020**, *41* (1), 50−53.
(27) Choi, S.; Jang, J.; Kang, H.; Baeck, J. H.; Bae, J. U.; Park, K. S.; Yoon, S. Y.; Kang, I. B.; Kim, D. M.; Choi, S. J.; Kim, Y. S.; Oh, S.; Kim, D. H. Systematic Decomposition of the Positive Bias Stress Instability in Self-Aligned Coplanar InGaZnO Thin-Film Transistors. *IEEE Electron Device Lett.* **2017**, *38* (5), 580−583.
(28) Huang, B. S.; Chang, T. C.; Tai, M. C.; Chang, H. Y.; Zhou, K. J.; Sun, L. C.; Huang, J. W.; Chen, M. C.; Huang, H. C. Abnormal Hump and Two-Step Degradation of Top Gate a-InGaZnO TFTs Under Positive Bias Stress. *IEEE Trans. Electron Devices* **2022**, *69* (8), 4288−4292.
(29) Jin, J. W.; Nathan, A.; Barquinha, P.; Pereira, L.; Fortunato, E.; Martins, R.; Cobb, B. Interpreting anomalies observed in oxide semiconductor TFTs under negative and positive bias stress. *AIP Adv.* **2016**, *6* (8), 085321.
(30) Fleetwood, D. M.; Winokur, P. S.; Reber, R. A., Jr; Meisenheimer, T. L.; Schwank, J. R.; Shaneyfelt, M. R.; Riewe, L. C. Effects of oxide traps, interface traps, and "border traps" on metal-oxide-semiconductor devices. *J. Appl. Phys.* **1993**, *73* (10), 5058−5074.
(31) Kim, Y. G.; Kim, T.; Avis, C.; Lee, S. H.; Jang, J. Stable and High-Performance Indium Oxide Thin-Film Transistor by Ga Doping. *IEEE Trans. Electron Devices* **2016**, *63* (3), 1078−1084.
(32) Lee, S.; Koo, B.; Shin, J.; Lee, E.; Park, H.; Kim, H. Effects of hydroxyl groups in polymeric dielectrics on organic transistor performance. *Appl. Phys. Lett.* **2006**, *88* (16), 162109.
(33) Abbas, S.; Kumar, M.; Ban, D. K.; Yun, J. H.; Kim, J. Transparent and Flexible In2O3 Thin Film for Multilevel Nonvolatile Photomemory Programmed by Light. *ACS Appl. Electron. Mater.* **2019**, *1* (3), 437−443.
(34) Wang, C.; Lu, W. M.; Li, F. N.; Ning, H. Y.; Ma, F. Persistent photoconductivity in a-IGZO thin films induced by trapped electrons and metastable donors. *J. Appl. Phys.* **2022**, *131* (12), 125709.
(35) Yin, Z. G.; Zhang, X. W.; Fu, Z.; Yang, X. L.; Wu, J. L.; Wu, G. S.; Gong, L.; Chu, P. K. Persistent photoconductivity in ZnO nanostructures induced by surface oxygen vacancy. *Phys. Status Solidi RRL* **2012**, *6* (3), 117−119.
(36) Gao, S. L.; Qiu, L. P.; Zhang, J.; Han, W. P.; Ramakrishna, S.; Long, Y. Z. Persistent Photoconductivity of Metal Oxide Semiconductors. *ACS Appl. Electron. Mater.* **2024**, *6* (3), 1542−1561.
(37) Sun, M.; Gao, R. T.; He, J. L.; Liu, X. H.; Nakajima, T.; Zhang, X. Y.; Wang, L. Photo-driven Oxygen Vacancies Extends Charge Carrier Lifetime for Efficient Solar Water Splitting. *Angew. Chem., Int. Ed.* **2021**, *60* (32), 17601−17607.

https://doi.org/10.1021/acsaelm.5c01021
ACS Appl. Electron. Mater. 2025, 7, 6187−6195